

Article

Bi₂Te₃ Topological Insulator for Domain-Wall Dark Pulse Generation from Thulium-Doped Fiber Laser

Joonhoi Koo ¹, Nandam Ashok ¹, Dong Hwan Kim ² and Woojin Shin ^{1,*}

¹ Advanced Photonics Research Institute, Gwangju Institute of Science and Technology, 123 Cheomdangwagi-ro, Buk-gu, Gwangju 61005, Korea

² Defence R&D Center, Hanwha Corporation, 305 Pangyo-ro, Bundang-gu, Seongnam-si, Gyeonggi-do 13488, Korea

* Correspondence: swj6290@gist.ac.kr; Tel.: +82-62-715-3343

Received: 31 May 2019; Accepted: 28 June 2019; Published: 29 June 2019



Abstract: We have experimentally demonstrated domain-wall (DW) dark pulses from a thulium-doped fiber laser incorporating a topological insulator saturable absorber (SA). The bulk-structured Bi₂Te₃ was used as the SA, which was constructed on a fiber ferrule platform through the deposition of the Bi₂Te₃ mixed with distilled water. The DW dark pulses were generated from the thulium-doped fiber laser cavity with a dual wavelength at 1956 nm and 1958 nm. The dark pulse width and the repetition rate were measured as ~10.3 ns and ~20.7 MHz over the pump power of ~80 mW, respectively. To the best of our knowledge, this work is the first demonstrated generation of the DW dark pulse from a thulium-doped fiber laser using nanomaterial-based SA.

Keywords: Bi₂Te₃; topological insulator; domain-wall dark pulses; fiber lasers

1. Introduction

Optical soliton has been seen as an attractive physical system for optical communication, optical signal processing system and the formation of an ultra-short pulse within a laser cavity [1–3]. Most of the previously reported works have been discovered through the soliton mode-locking operation of lasers in a bright pulse regime over certain periods of time [1–5]. In addition to the traditional soliton, dark solitons also exist, which operate in a negative pulse regime.

In 1987, the dark soliton was first experimentally reported within a single mode optical fiber by Emplit et al. [6]. After that, theoretical and experimental studies have been intensively conducted in the last few decades [7–14]. It has been reported that the dark pulses are more stable and less sensitive to fibers in comparison to bright pulses [7]. The dark soliton relates to the nonlinear Schrödinger equation (NLSE). The dark pulse can be predicted using the NLSE [8]. The formation of the dark pulses is based on the following three mechanisms: NLSE dark pulse, cubic-quintic nonlinear Schrödinger equation (CQNLSE) dark pulse and domain-wall (DW) dark pulses [8–15].

Among the dark pulses, the DW dark pulse is based on multi-wavelength lasing and causes topological defects in the time domain. Compared with the NLSE dark pulse, DW dark pulses can be generated regardless of cavity dispersion regions [16]. In addition, it is well known that the formation of DW dark pulses can be more compact compared to CQNLSE-type dark pulses since they can be generated without a highly nonlinear optical medium [16]. Recently, such DW dark pulse lasers from fiber lasers have been investigated using nanomaterial-based saturable absorbers (SAs), such as carbon nanotube, topological insulators (TIs) and transition metal dichalcogenides (TMDs) [16–21].

Among the nanomaterials, the TI, as the new Dirac material, has a unique conducting surface, which is topologically protected against scattering by time-reversal symmetry and insulating energy gaps in bulk [22–24]. With such a unique physical characteristic, TI has gained huge scientific and

technical attention in the field of condensed matters for spintronics and quantum device [24,25]. Apart from the field of condensed matters, a number of demonstrations have been also carried out in field of photonics for the use of TI-based SA for recent years. After this, the great performance of the TI-based SA for pulsed fiber lasers has been demonstrated due to its nonlinear absorption and fast recovery time [17,26,27].

The aim of this study was to experimentally demonstrate the DW dark pulse in the 1950-nm region from a thulium-doped fiber (TDF) laser cavity using the nanomaterial-based SA. Although the DW dark pulse generation has been already demonstrated using the nanomaterial-based SA, the previously reported works have been only conducted with ytterbium-doped and erbium-doped fiber lasers in the 1064-nm and 1550-nm regions [16–21]. Thus, we thought that it would be technically meaningful to investigate the DW dark pulse in the 1950-nm region.

A Bi_2Te_3 TI was chosen as a SA in this work among the TI-based SAs because it has broad saturable absorption that has a small band gap (0.2–0.3 eV) and falls within mid-infrared region [26]. By using the Bi_2Te_3 TI SA, the DW dark pulse was readily generated from the thulium-doped fiber laser cavity according to the particular polarization state within the cavity. The dark pulse width and repetition rate of the generated dark pulse were measured at ~ 10.3 ns and 20.7 MHz, respectively. The signal-to-noise (SNR) ratio of the pulses was ~ 55.5 dB. To the best of our knowledge, this is the first demonstrated generation of the DW dark pulse from a thulium-doped fiber laser in the 1956-nm region using nanomaterial-based SA.

2. Materials and Methods

The SA used in this work was prepared by dropping a small amount of a mixed solution containing Bi_2Te_3 and distilled water onto the end surface of a FC/PC fiber ferrule. We first prepared the commercially available bulk-structured Bi_2Te_3 powder to fabricate the SA (Sigma Aldrich, Bi_2Te_3 metal basis). Bi_2Te_3 was characterized through scanning electron microscopy (SEM, S-4700, Hitachi, Tokyo, Japan) and energy dispersive spectroscopy (EDS, 7200-H, Horiba, Kyoto, Japan). Figure 1 shows the measured image of Bi_2Te_3 powder. Its size is randomly variable from ~ 0.7 μm to ~ 30 μm , which shows that the prepared powder is bulk-structured. The measured EDS spectrum is shown in Figure 1b. Both strong Bi and Te peaks are clearly evident while tiny C peaks are observable due to the use of carbon tape for attaching Bi_2Te_3 powder into powder holders for SEM. The atomic ratio of both Bi and Te was measured as 31.29% and 20.67%, which indicates that the ratio between Bi and Te is nearly 2:3.

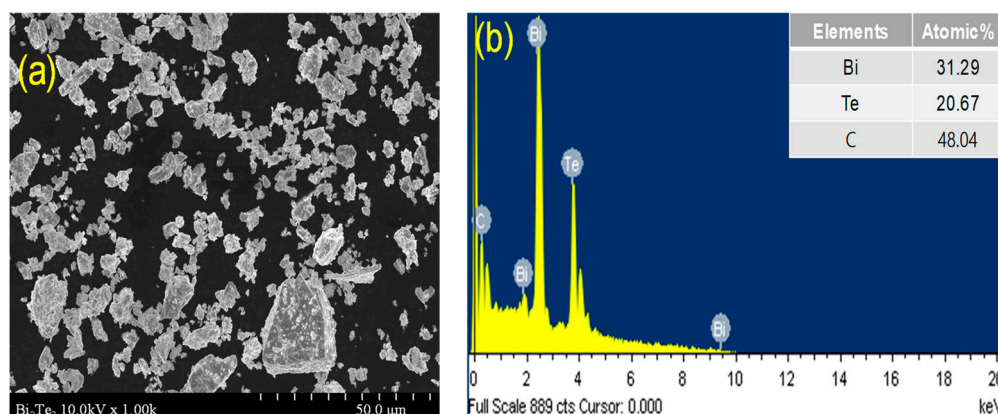


Figure 1. Measured (a) SEM image and (b) EDS spectrum of the Bi_2Te_3 powder used in this work.

To form Bi_2Te_3 film for the Bi_2Te_3 -based SA, the Bi_2Te_3 powder is mixed with 2 ml of distilled water without any post-processing, such as ultrasonication and stirring with mechanical facility. Next, the solution is dropped on the facet of the ferrule and left to dry for 24 hours. Figure 2 shows actual photos of the Bi_2Te_3 solution and the Bi_2Te_3 film sitting onto the fiber ferrule. Although we did not use

an organic solvent to fabricate the Bi_2Te_3 solution, it was enough for the Bi_2Te_3 -mixed Bi_2Te_3 to form distilled water film onto the ferrule, as shown in Figure 2b.

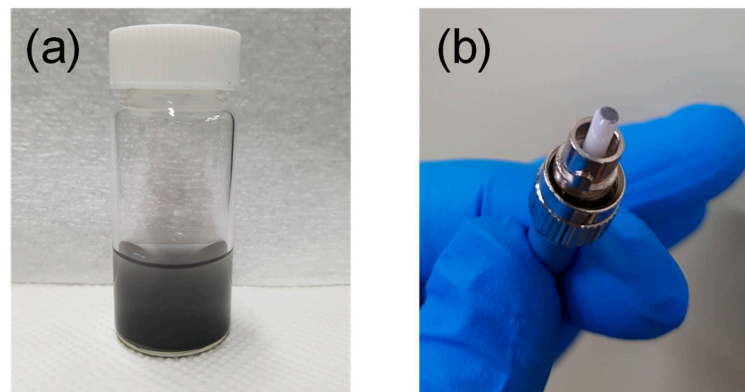


Figure 2. Real photograph of (a) the Bi_2Te_3 solution and (b) the Bi_2Te_3 film onto the fiber ferrule.

Figure 3 shows the connecting schematic diagram of the Bi_2Te_3 SA. Before connecting the two fiber ferrules, the index matching gel (G608N, Thorlabs, Newton, NJ, USA) was dropped on the top of another ferrule to reduce scattering loss and to ensure the firm fixation of the Bi_2Te_3 particles between the fiber ferrules [28]. Both FC/PC ferrules were connected with the FC/PC fiber ferrule adaptor, as shown in Figure 3b. Its insertion loss was measured as ~ 4 dB at $1.9 \mu\text{m}$.

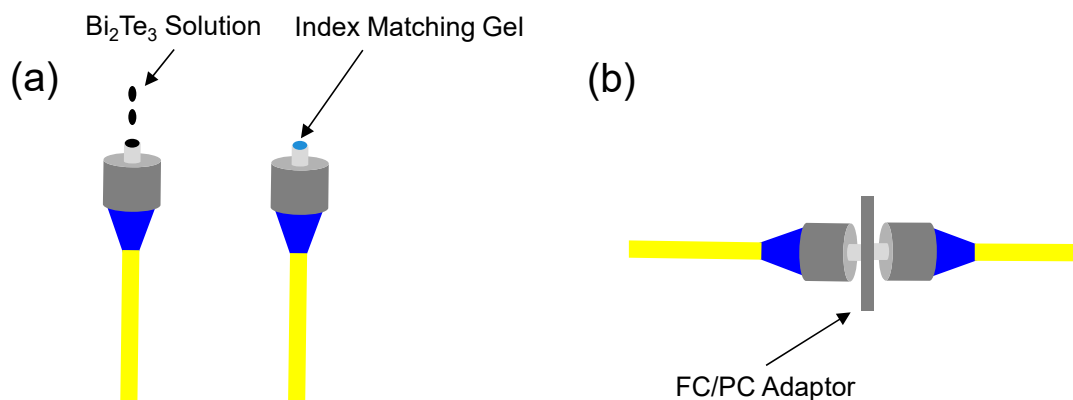


Figure 3. (a) The prepared fiber ferrules. (b) The connecting schematic diagram of the Bi_2Te_3 SA.

The nonlinear transmission of the prepared SA was also measured using lab-made, ~ 1.5 ps fiber laser with a repetition rate of 24 MHz at $1.93 \mu\text{m}$. Figure 4 shows the measured nonlinear transmission with a fitted curve [27]:

$$T(I) = 1 - \Delta T \cdot \exp\left(\frac{-I}{I_{sat}}\right) - T_{ns} \quad (1)$$

where T is the transmission, ΔT is the modulation depth, I is the incident-pulse energy, I_{sat} is the saturation energy and T_{ns} is the nonsaturable loss. The modulation depth and saturation intensity were measured as $\sim 1.3\%$ and 36 MW/cm^2 , respectively. Although the modulation depth of the fabricated SA is slightly low, it is enough to induce DW dark pulses in this work.

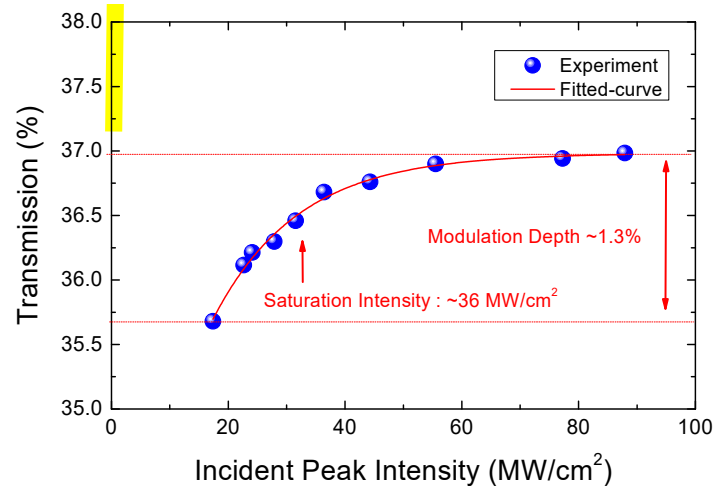


Figure 4. Measured nonlinear transmission of the Bi₂Te₃ SA.

3. Results and Discussion

The prepared SA was subsequently inserted within TDF ring cavity, as shown in Figure 5. A 3-m TDF (TMDF200, OFS, Norcross, GA, USA) was used as the gain medium. The TDF was pumped by a 1560-nm laser diode via the 1560/1950-nm wavelength division multiplexer (WDM). The output power was extracted by the 20% port of a 20:80 optical coupler. For the unidirectional light propagation, an optical isolator was used. A polarization controller (PC) was used to adjust polarization states within the cavity. The SA was located between the coupler and isolator. The total cavity length was measured as ~9.5 m and its cavity group velocity dispersion (GVD) was calculated as -0.64 ps² according to the previously measured dispersion values [29,30]. The laser output was measured by an optical spectrum analyzer (AQ6375, Yokogawa, Tokyo, Japan) a 500-MHz oscilloscope (6050A, Lecroy, Chestnut Ridge, NY, USA), with a 10-GHz photodetector (ET-5010F, EOT, Traverse City, MI, USA), an electrical spectrum analyzer (USB-SA124B, Signalhound, Battle Ground, WA, USA), and an autocorrelator (FR-103MN, Femtochrome Research, Berkeley, CA, USA).

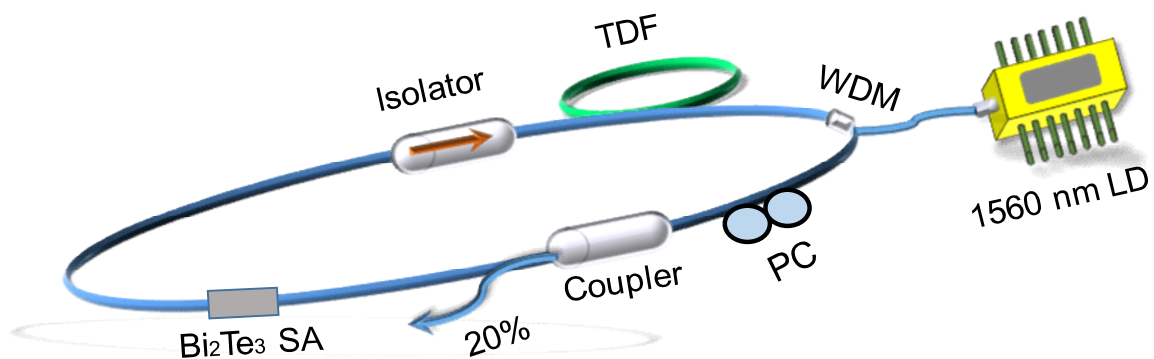


Figure 5. Experimental set-up for the thulium-doped fiber cavity.

We increased the pump power and the laser operated in continuous wave (CW) mode at a pump power of ~58 mW. When the pump power reached 80 mW, the laser generated dark pulses according to polarization state within the cavity. It should be noted that the laser operated in CW mode without the proposed SA. The cavity generated two wavelengths of 1956 nm and 1958 nm, as shown in Figure 6a. The dual-wavelength operation of the laser induced the topological defects in the temporal domain with a narrow dip in the background of its CW output, as shown in Figure 6b. The negative pulse width and repetition rate were measured as ~10.3 ns and 20.7 MHz, respectively. The autocorrelation was also measured although no peaks were observed. The dark pulse was generated until the pump power reached 120 mW in the 1956-nm region. At a pump power of 120 mW, the dark pulse was

not generated from the laser cavity and the laser operated in CW mode. As the polarization state within the laser cavity was adjusted, the wavelength of the laser output was changed from 1940 nm to 1965 nm. However, the dark pulse operation of the laser was only observed near the 1950-nm region.

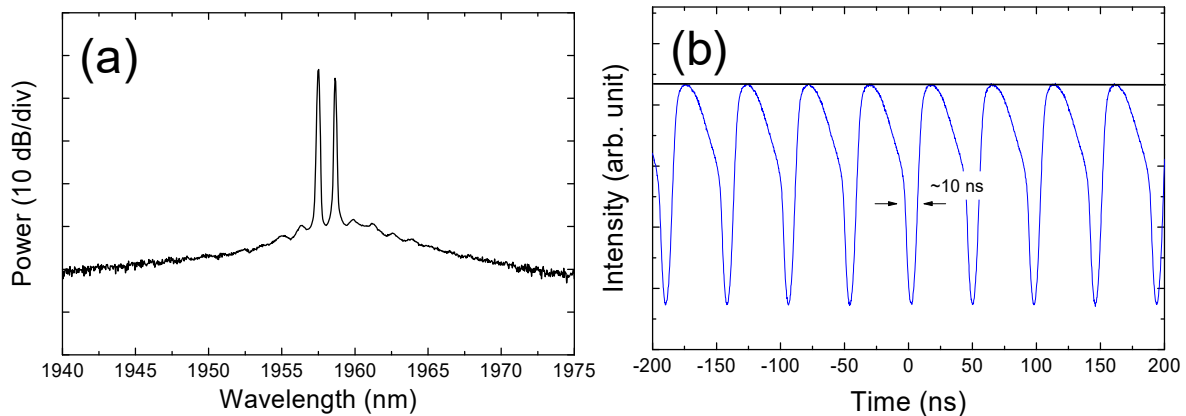


Figure 6. Measured (a) optical spectrum and (b) oscilloscope traces of the dark pulses.

After this, the electrical spectrum of the laser output was measured, as shown in Figure 7. Figure 7a shows the 1-MHz span of the electrical spectrum. The strong single peak was observed at the center frequency of ~ 20.7 MHz with a SNR of ~ 55 dB although the laser operated at a dual wavelength. Here, the single peak shows that the laser operates in DW condition whereby the mutual coupling of the dual wavelength induces a single frequency component, as previously reported in reference [16]. The wide span of electrical spectrum is also shown in Figure 7b.

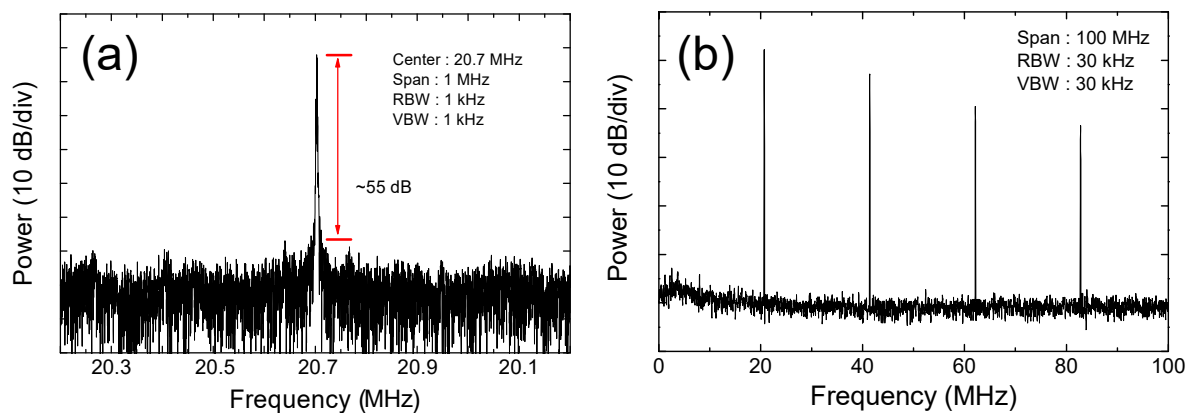


Figure 7. Measured electrical spectra of the dark pulses: (a) narrow span and (b) wide span.

The DW dark pulse in this work was generated in an anomalous dispersion cavity. We were unable to check the generation of the DW dark pulse under a normal dispersion regime due to the lack of normal dispersion fibers in our laboratory. It is estimated that the similar DW dark pulse can be generated from normal dispersion cavity under the same conditions in this work because the DW dark pulse can be generated regardless of dispersion regime [16]. However, further investigation focusing on the effect of dispersion on the generation of the DW dark pulse is needed.

4. Conclusions

In conclusion, we have experimentally demonstrated DW dark pulses in the 1956-nm wavelength region from a thulium-doped fiber laser using the bulk-structured Bi_2Te_3 SA. The pulse width and repetition rate of dark pulses were measured as 10.3 ns and 20.7 MHz, respectively. To the best of our knowledge, the experimental results are the first demonstrated results for the generation of DW dark

pulses from a thulium-doped fiber laser using nanomaterial-based saturable absorbers, such as TIs, carbon nanomaterials and TMDs.

We believe that our experimental results could further improve the understanding of DW dark pulse generation in the 1950-nm region.

Author Contributions: Formal analysis, J.K.; Methodology, J.K.; Writing—Original Draft, J.K. and N.A.; Writing—Review and Editing, D.H.K. and W.S.

Funding: This work was supported by Optical Fiber Laser Innovation Research and Development Project, funded by Hanwha Corporation.

Acknowledgments: The authors would like to thank K. Jeong for his experimental assistance at APRI.

Conflicts of Interest: The authors declare no conflict of interest.

References

1. Mikulla, B.; Leng, L.; Sears, S.; Collings, B.C.; Arend, M.; Bergman, K. Broad-band high-repetition-rate source for spectrally sliced WDM. *IEEE Photon. Technol. Lett.* **1999**, *11*, 418–420. [[CrossRef](#)]
2. McFerran, J.J. Échelle spectrograph calibration with a frequency comb based on a harmonically mode-locked fiber laser: A proposal. *Appl. Opt.* **2009**, *48*, 2752–2759. [[CrossRef](#)] [[PubMed](#)]
3. Carruthers, T.F.; Duling, I.N. 10-GHz, 1.3-ps erbium fiber laser employing soliton pulse shortening. *Opt. Lett.* **1996**, *21*, 1927–1929. [[CrossRef](#)] [[PubMed](#)]
4. Tiu, Z.C.; Tan, S.J.; Zarei, A.; Ahmad, H.; Harun, S.W. Nonlinear polarization rotation-based mode-locked Erbium-doped fiber laser with three switchable operation states. *Chin. Phys. Lett.* **2014**, *31*, 094206. [[CrossRef](#)]
5. Eckstein, J.N.; Ferguson, A.I.; Hänsch, T.W. High-resolution two-photon spectroscopy with picosecond light pulses. *Phys. Rev. Lett.* **1978**, *40*, 847–850. [[CrossRef](#)]
6. Emplit, P.; Hamaide, J.P.; Reynaud, F.; Froehly, C.; Barthelemy, A. Picosecond steps and dark pulses through nonlinear single mode fibers. *Optics Communication.* **1987**, *62*, 374–379. [[CrossRef](#)]
7. Agrawal, G.P. *Nonlinear Fiber Optics*, 3rd ed.; Academic Press: San Diego, CA, USA, 2001.
8. Zakharov, V.E.; Shabat, A.B. Interaction between solitons in a stable medium. *Soviet Phys.* **1973**, *37*, 823–828.
9. Tang, D.Y.; Li, L.; Song, Y.F.; Zhao, L.M.; Zhang, H.; Shen, D.Y. Evidence of dark solitons in all-normal-dispersion-fiber lasers. *Phys. Rev. A.* **2013**, *88*, 013849. [[CrossRef](#)]
10. Zian, C.T.; Arman, Z.; Sin, J.T.; Harith, A.; Sulaiman, W.H. Harmonic dark pulse emission in erbium-doped fiber laser. *Chin. Phys. Lett.* **2015**, *32*, 034203. [[CrossRef](#)]
11. Zhang, H.; Tang, D.Y.; Zhao, L.M.; Wu, X. Dark pulse emission of a fiber laser. *Phys. Rev. A* **2009**, *80*, 045803. [[CrossRef](#)]
12. Zhang, H.; Tang, D.Y.; Zhao, L.M.; Knize, R.J. Vector dark domain wall solitons in a fiber ring laser. *Opt. Express* **2010**, *18*, 4428–4433. [[CrossRef](#)] [[PubMed](#)]
13. Malomed, B.A. Domain wall between traveling waves. *Phys. Rev. E.* **1994**, *50*, R3310–R3313. [[CrossRef](#)]
14. Malomed, B.A. Optical domain walls. *Phys. Rev. E* **1994**, *50*, 1565–1571. [[CrossRef](#)]
15. Tiu, Z.C.; Suthaskumar, M.; Zarei, A.; Tan, S.J.; Ahmad, H.; Harun, S.W. Generation of switchable domain wall and cubic–quintic nonlinear Schrödinger equation dark pulse. *Opt. Laser Technol.* **2015**, *73*, 127–129. [[CrossRef](#)]
16. Ahmad, H.; Tiu, Z.; Zarei, A.; Suthaskumar, M.; Salim, M.A.M.; Harun, S.W. Domain-wall dark pulse generation in fiber laser incorporating MoS₂. *Appl. Phys. B.* **2016**, *122*, 69–73. [[CrossRef](#)]
17. Liu, J.; Li, X.; Zhang, S.; Zhang, H.; Yan, P.; Han, M.; Pang, Z.; Yang, Z. Polarization domain wall pulses in a microfiber-based topological insulator fiber laser. *Sci. Rep.* **2016**, *6*, 29128. [[CrossRef](#)] [[PubMed](#)]
18. Guo, B.; Yao, Y.; Xiao, J.J.; Wang, R.L.; Zhang, J.Y. Topological insulator-assisted dual-wavelength fiber laser delivering versatile pulse patterns. *IEEE J. Sel. Top. Quantum Electron.* **2016**, *22*, 0900108. [[CrossRef](#)]
19. Markom, A.M.; Tan, S.J.; Haris, H.; Paul, M.C.; Dhar, A.; Das, S.; Harun, S.W. Experimental Observation of Bright and Dark Solitons Mode-Locked with Zirconia-Based Erbium-Doped Fiber Laser. *Chin. Phys. Lett.* **2018**, *35*, 024203. [[CrossRef](#)]
20. Liu, H.; Chow, K. Dark pulse generation in fiber lasers incorporating carbon nanotubes. *Opt. Express.* **2014**, *22*, 29708–29713. [[CrossRef](#)]

21. Zhao, J.; Wang, Y.; Yan, P. An L-band graphene-oxide mode-locked fiber laser delivering bright and dark pulses. *Laser Phys.* **2013**, *23*, 075105. [[CrossRef](#)]
22. Xiu, F.; He, L.; Wang, Y.; Cheng, L.; Chang, L.T.; Lang, M.; Huang, G.; Kou, X.O.; Zhou, Y.; Jiang, X.; et al. Manipulating surface states in topological insulator nanoribbons. *Nat. Nano.* **2011**, *6*, 216–221. [[CrossRef](#)] [[PubMed](#)]
23. Hong, M.; Chasapis, T.C.; Chen, Z.G.; Yang, L.; Kanatzidis, M.G.; Snyder, G.J.; Zou, J. n-Type Bi₂Te_{3-x}Se_x Nanoplates with Enhanced Thermoelectric Efficiency Driven by Wide-Frequency Phonon Scatterings and Synergistic Carrier Scatterings. *ACS Nano.* **2016**, *10*, 4719–4727. [[CrossRef](#)] [[PubMed](#)]
24. Wang, K.; Liu, Y.; Wang, W.; Meyer, N.; Bao, L.H.; He, L.; Lang, M.R.; Chen, Z.G.; Che, X.Y.; Post, K.; et al. High-quality Bi₂Te₃ thin films grown on mica substrates for potential optoelectronic applications. *Appl. Phys. Lett.* **2013**, *103*, 031605.
25. Koo, J.; Lee, J.; Chi, C.; Lee, J.H. Passively Q-switched 1.56 μm all-fiberized laser based on evanescent field interaction with bulk-structured bismuth telluride topological insulator. *J. Opt. Soc. Am. B* **2014**, *31*, 2157–2162. [[CrossRef](#)]
26. Lee, J.; Koo, J.; Jhon, Y.M.; Lee, J.H. A femtosecond pulse erbium fiber laser incorporating a saturable absorber based on bulk-structured Bi₂Te₃ topological insulator. *Opt. Express.* **2014**, *22*, 6165–6173. [[CrossRef](#)] [[PubMed](#)]
27. Chen, Y.; Zhao, C.; Chen, S.; Du, J.; Tang, P.; Jiang, G.; Zhang, H.; Wen, S.; Tang, D. Large energy, wavelength widely tunable, topological insulator Q-switched erbium-doped fiber laser. *IEEE J. Sel. Top. Quantum Electron.* **2014**, *20*, 0900508.
28. Lee, J.; Lee, J.; Koo, J.; Lee, J.H. Graphite saturable absorber based on the pencil-sketching method for Q-switching of an erbium fiber laser. *Appl. Opt.* **2016**, *55*, 303–309. [[CrossRef](#)] [[PubMed](#)]
29. Kharitonov, S.; Billat, A.; Brès, C.-S. Kerr nonlinearity and dispersion characterization of core-pumped thulium-doped fiber at 2 μm. *Opt. Lett.* **2016**, *41*, 3173–3176. [[CrossRef](#)] [[PubMed](#)]
30. Ciągła, P.; Rampur, A.; Heidt, A.; Feurer, T.; Klimczak, M. Dispersion measurement of ultra-high numerical aperture fibers covering thulium, holmium, and erbium emission wavelengths. *J. Opt. Soc. Am. B* **2018**, *8*, 1301–1307. [[CrossRef](#)]



© 2019 by the authors. Licensee MDPI, Basel, Switzerland. This article is an open access article distributed under the terms and conditions of the Creative Commons Attribution (CC BY) license (<http://creativecommons.org/licenses/by/4.0/>).